Journal of Aerosol Science 76 (2014) 138–147

Contents lists available at ScienceDirect

Journal of Aerosol Science

journal homepage: www.elsevier.com/locate/jaerosci

Coagulation of charged particles in self-organizing thermal plasmas of welding fumes

V.I. Vishnyakov *, S.A. Kiro, M.V. Oprya, A.A. Ennan

Physical–Chemical Institute for Environmental and Human Protection, National Academy of Sciences of Ukraine, 3 Preobrazhenskaya, Odessa 65082, Ukraine

ARTICLE INFO

Article history:
Received 25 April 2014
Received in revised form
13 June 2014
Accepted 25 June 2014
Available online 1 July 2014

Keywords:
Thermal plasma
Self-organization
Welding fume
Primary particles
Ordered structures
Coagulation

ABSTRACT

The dusty plasma behavior is studied in the process of coagulation of the primary particles, which are formed as a result of the nucleation and nuclei growth in the condensable high-temperature vapors. The study is concentrated to the example of the thermal plasma formed in the welding fume in the arc welding process where the electrodes covered with carbonate–fluorite are used. The tendency to self-organization of such a plasma and formation of the ordered spatial structures of primary particles is demonstrated. The number densities of the primary particles in these structures are much higher than at uniform spatial distribution that causes the rapid coagulation of the fine nano-sized primary particles. The coagulation of the particles with size more 10 nm into cluster-like agglomerates occurs during almost all cooling period of aerosol up to the ambient air temperature. The coagulation of the ultra-fine particles (~2 nm) occurs in two stages: at first the chain-like agglomerates are formed rapidly, and then they associate with the cluster-like agglomerates. As a result, the final agglomerates (inhalable particles) have the bimodal size distribution with different chemical compositions and fractal dimensions.

1. Introduction

The common name “dusty plasma” is referred to a wide range of heterogeneous physical systems, in which the ionized gas environment and suspended solid or liquid particles are present simultaneously. In some kinds of dusty plasmas the particles are formed as a result of the metal (metal compound) vapors' condensation, in others – as a result of the cluster coagulation or the gas and construction material interaction. In any case, formation of the dust component is accompanied by coagulation of the fine particles and modification of the dust size distribution.

The basic property of dusty plasmas is the charging of particles by the interphase interaction. Dependency of the particles' coagulation on their charge was studied by some authors, for example by Belov, Ivanov, Pal, Ryabinkin, and Serov (2002), Ivlev, Morfill, and Konopka (2002), Nguyen and Shklovskii (2002), Olevanov, Mankelevich, and Rakhimova (2004), Mankelevich et al. (2009). In particular, the collision frequency that corresponds to the thermal cross-section for the interaction between dust particles cannot account for such a high cluster growth rate observed experimentally (Bouchoule et al., 1996). The anomalously high coagulation rate is explained by assuming that collisions take place mostly between oppositely charged particles (Watanabe, 2006). Another approach is demonstrated by Olevanov et al. (2004), where the

* Corresponding author. Tel.: +380 487237528; fax: +380 487231116.
E-mail addresses: drvishnyakov@mail.ru, eksvar@ukr.net (V.I. Vishnyakov).

http://dx.doi.org/10.1016/j.jaerosci.2014.06.010
0021-8502/

polarization model for the interaction between dust particles is considered. On the other hand, some authors note that a coagulation rate of the likely charged dust is less than for neutral dust; the calculations, which demonstrate the absence of aggregates' growth as a result of coagulation of the likely charged particles, are given by Smith, Lee, and Matsoukas (1999) and Belov et al. (2000). It is explained by the obvious Coulomb repulsion of the dust particles. Thus, the general theory of the charged dust particles coagulation in the plasma is absent, but it is possible to assume that all noted above effects can be present at the certain stages of the plasma dust coagulation.

A variety of mechanisms of the dust particle collisions cause the different morphological types of the agglomerates in the plasma. For example, the linear chain morphology has been observed in iron particles contained in the plasma of welding fumes (Zimmer & Biswas, 2001). Three morphological types of the agglomerates in welding fumes have been observed by Sowards, Ramirez, Dickinson, and Lippold (2010), Berlinger et al. (2011) and Oprya et al. (2012): the cluster-like agglomerates (densely or loosely packed spherical particles), the chain-like agglomerates with fractal geometry, and the coarse particles on which chain-like agglomerates are located. The mechanisms of the various morphology types' formation are not clear and need to be investigated.

It should be noted that attraction or repulsion of the dust particles in the plasma is determined by their interaction with the environment rather than by their charges. The situation when the likely charged particles are attracted is possible in the plasma. The source of attractive force is the ion drag force in the low-pressure collisionless plasma (Khrapak, Ivlev, Morfill, & Thomas, 2002), or the ion diffusion pressure force in the high-pressure collision plasma (Vishnyakov, 2005). The possibility of the long-range attraction between likely charged particles leads to the self-organization of dusty plasmas and to the formation of the spatial ordered structures such as the plasma crystals (Morfill, Thomas, Konopka, & Zuzic, 1999, 2004; Fortov, Khrapak, Khrapak, Molotkov, & Petrov, 2004).

In the paper by Olevanov, Mankelevich, and Rakhimova (2003) it has been noted that there exist two different types of the interaction between the particles in dusty plasmas: the first type is the formation of plasma crystals, and the second type is the particle coagulation. In the present paper the plasma self-organization and the coagulation are studied simultaneously, because the self-organization causes the accumulation of the fine particles in the small space area (Vishnyakov & Dragan, 2006), i.e. their local number density can be increased. It should lead to the increase of Brownian coagulation rate.

2. Conditions of the collision plasma self-organization

The self-organization of the thermal collision dusty plasma, to which the combustion plasma and the plasma of welding fumes belong, occurs due to the displacement of ionization balance near surfaces of the charged dust particles (Vishnyakov, 2005, 2006). The change of the electron number density in the space charge layer near a particle surface occurs as a result of the electrical interaction, and the balance between the thermal ionization of atoms and the electron–ion recombination are broken. It leads to occurrence of the nonequilibrium charge carriers whose spatial distribution is not determined by the Boltzmann factor. And, the plasma ionization is increased near a positive particle, but is decreased near negative particles.

The conservation of the nonequilibrium carrier number density δn is determined by the continuity equation, which in the stationary case reads

$$-D\nabla^2\delta n=\beta_I n_a(n_e+\delta n)-\gamma_R(n_e+\delta n)(n_i+\delta n),$$

where $D=2D_eD_i/(D_e+D_i)$ is the ambipolar diffusion coefficient; β_I is the ionization rate; γ_R is the recombination rate; n_a is the ionizable atom number density; n_e and n_i are the equilibrium electron and ion number densities respectively.

The flux of the nonequilibrium charge carriers to the particle surface can be obtained via solving this equation (Vishnyakov, 2005):

$$j_s=\frac{Dn_q}{r_D}\frac{\exp\frac{V_b}{k_BT}-1}{\sqrt{2\cosh\frac{V_b}{k_BT}-1}}, \tag{1}$$

where $r_D=\sqrt{k_BT/8\pi e^2n_0}$ is the screening length; V_b is the potential barrier at the particle surface; k_B is the Boltzmann constant; T is the Kelvin temperature; n_0 and n_q are the unperturbed and quasiunperturbed number densities (discussed below).

The flux (1) determines the attractive force between likely charged particles in the thermal plasma. The repulsing occurs due to the electrical force. Existence of the competitive forces is the condition for the ordered structures formation (Vishnyakov & Dragan, 2006).

The attractive force between the likely charged particles, in reality, is the force which acts on the particles from the plasma and pushes these particles to each other contrary to the electrical forces. Such a pushing appears when the nonequilibrium carriers are distributed anisotropically around the particle. The total momentum, which is transferred from the flux of nonequilibrium positive ions to the particles by collisions, pulls particles together, when the ionization degree in the layer between negative particles is less than outside. The positive charge of the particles causes the increase of ionization degree and in the layer between particles it becomes larger than outside. But the field in this case suppresses the collisions of ions with particles and the excess momentum occurs due to the collisions with atoms whose number in the

ambient medium exceeds that between the particles. As a result, the anisotropic momentum transfer to the particle surface by the flux of the nonequilibrium carriers (1) ensures the existence of the average force of the ion pressure:

$$\mathbf{F}_P = \frac{m_i D^2}{r_D \lambda_R} \frac{\exp\frac{V_b}{k_B T} - 1}{\sqrt{2\cosh\frac{V_b}{k_B T} - 1}} \int_S n_q \, d\mathbf{s}, \tag{2}$$

where m_i is the ion mass; $\lambda_R = \sqrt{D/\gamma_R n_0}$ is the recombination length; and S is the particle surface.

The unperturbed number density n_0 is the number density of ions and electrons far from the dust particles, where the plasma is neutral ($n_e = n_i = n_0$), and this number density corresponds to the equilibrium ionization, which is described by the Saha equation (Landau & Lifshitz, 1976):

$$\frac{n_0^2}{n_a} = \frac{\Sigma_i}{\Sigma_a} \nu_e \exp\frac{-I}{k_B T} \equiv K_S, \tag{3}$$

where $n_a = n_A - n_i$ is the equilibrium number density of ionizable atoms as a result of thermal ionization; n_A is the initial number density of ionizable atoms; Σ_i and Σ_a are the statistical weights of ions and atoms respectively; $\nu_e = 2(m_e k_B T/2\pi\hbar^2)^{3/2}$ is the effective density of the electron states; m_e is the electronic mass; $\hbar$ is the Plank constant; I is the ionization potential of the ionizable atoms (alkali-metal); and K_S is the Saha constant.

The quasiunperturbed number density describes the nonequilibrium ionization:

$$\frac{n_q^2}{n_a} = K_S \exp\frac{-e\varphi_{pl}}{k_B T}, \tag{4}$$

where φ_{pl} is the bulk plasma potential which is additive to the potential of ionization $I_{eff} = I + e\varphi_{pl}$ in the space charge layer (Vishnyakov, 2004; Vishnyakov & Dragan, 2005). The bulk plasma potential characterizes the size of operation that is necessary for the plasma to gain some volumetric charge as a result of interphase interaction. The local value of the bulk plasma potential is defined by the potential barrier on the plasma–particle boundary,

$$\varphi_{pl} = -2\frac{k_B T}{e} \tanh\frac{V_b}{4k_B T}. \tag{5}$$

The perturbation, caused by the particle in the plasma, decays with the distance from its surface (Vishnyakov & Dragan, 2006). For a spherical particle with radius a the dumping is determined as $\varphi_{pl}(r) = \varphi_{pl}^s a/r$, where φ_{pl}^s is the local value near the particle surface (5). As a result, from Eqs. (3)–(5) it follows for the quasiunperturbed number density:

$$n_q(r) = n_0 \exp\left(\frac{a}{r}\tanh\frac{V_b}{4k_B T}\right).$$

Then, the force of the ion pressure (2), which acts on the chosen particle j from other particles, is regulated by the following equation:

$$\mathbf{F}_P = C_P a_j^2 \frac{\exp\frac{V_{bj}}{k_B T} - 1}{\sqrt{2\cosh\frac{V_{bj}}{k_B T} - 1}} \sum_k \exp\left(\frac{a_k}{r_k}\tanh\frac{V_{bk}}{4k_B T}\right)\mathbf{e}_k, \tag{6}$$

where the constant $C_P = 4\pi m_i n_0 D^2/r_D\lambda_R$; r_k is the distance from the chosen particle to the kth neighboring particle; and $\mathbf{e}_k$ is the unit vector.

The resultant force is the difference between the force of the ion pressure (6) and the force of electrical interaction of the chosen particle j with each other particles k ($k \neq j$) is $F_{j,k} = F_{Pj,k} - eZ_j E_k$, where eZ_j is the charge of chosen particle. The field E_k created by the kth neighboring particle at the surface of the chosen particle can be described by the approximating equation from the paper by Vishnyakov & Dragan (2006):

$$F_E = Z_j \frac{2k_B T(r_k + r_D)\,\mathrm{sgn}(V_b)}{r_k r_D \sinh\left(\frac{a_k - r_k}{r_D} + \ln\left|\frac{a_k}{r_k}\tanh\frac{V_{bk}}{4k_B T}\right|\right)}. \tag{7}$$

The likely charged particles always repel each other under action of the force (7) and attract each other under action of the force (6) – the sign of expression before the sum in (6) is negative for negative particles, but the unit vector $\mathbf{e}_k < 0$ in this case. The situation is opposite for the unlikely charged particles: they attract each other under action of the electrical force (7) and repel each other under action of the force of the ion pressure (6). Therefore, the distance of the forces equilibrium R always exists.

In the weakly coupled plasma, Eqs. (6) and (7) can be linearized, and the resultant interaction force can be represented as

$$F_{j,k} \sim \frac{e^2 Z_j Z_k}{r_k}\left[\frac{\pi e^2 m_i n_0 D^2 a_j}{r_D \lambda_R (k_B T)^2} - \frac{1}{r_k}\exp\frac{a_k - r_k}{r_D}\right];$$

and hence it follows, that the equilibrium distance between particles (which corresponds to $F_{j,k}=0$) is determined mostly by the unperturbed number density, because $r_D \sim n_0^{-1/2}$ and $\lambda_R \sim n_0^{-1/2}$. Therefore, increase of the plasma ionization degree leads to decrease of the equilibrium distance.

3. Ordered spatial structures of the primary particles in the welding fume

Some examples of the ordered spatial structures of particles in the thermal dusty plasma are represented in paper by Vishnyakov & Dragan (2006). Here the welding fume, which is obtained when the electrodes covered with carbonate–fluorite Paton UONI 13/55 (American Welding Society classification E6015) are used (Ennan, Kiro, Oprya, & Vishnyakov, 2013), is considered as an environment for the possible formation of the ordered structures of the primary particles. As it follows from modeling by Vishnyakov, Kiro, & Ennan (2014b), the thermal plasma of the welding fume created by the single ionization of the alkali–metal atoms and by the electron emission from the dust particle surfaces is described, at the time of phase transition of the liquid droplets into the solid primary particles, by following parameters: the temperature $T=1770$ K; the unperturbed number density $n_0=5\times10^{13}$ cm^{-3}; the screening length $r_D=0.3$ μm; the recombination length $\lambda_R=0.06$ μm; and the ambipolar diffusion coefficient $D=1.9$ cm^2/s. The condensed phase of the plasma is characterized by the bimodal lognormal size distribution of the primary particles: the first mode contains particles with average diameter $d_1=2$ nm, standard deviation $\sigma_1=1.6$, average charge number $Z_1=-0.6$, and number density $n_{d1}=5.3\times10^{11}$ cm^{-3}; the second mode contains particles with average diameter $d_2=10$ nm, standard deviation $\sigma_2=2.1$, average charge number $Z_2=-2.5$, and number density $n_{d2}=6.6\times10^{12}$ cm^{-3}.

The results of computer simulation of the self-organization of the primary particles by the method of molecular dynamics are presented in Fig. 1. The number density of the second-mode particles ensures the average distance between particles of $2\sqrt[3]{3/4\pi n_{d2}}=0.66$ μm, when they have uniform spatial distribution. But under action of the forces (6) and (7) the second-mode particles form the plasma crystal with the lattice constant of $R_2\sim0.25$ μm, that is equivalent to the change of their number density up to $n_{d2}^{*}\sim10^{14}$ cm^{-3}. Thus, the self-organization of the second-mode particles increases their local number density ten times.

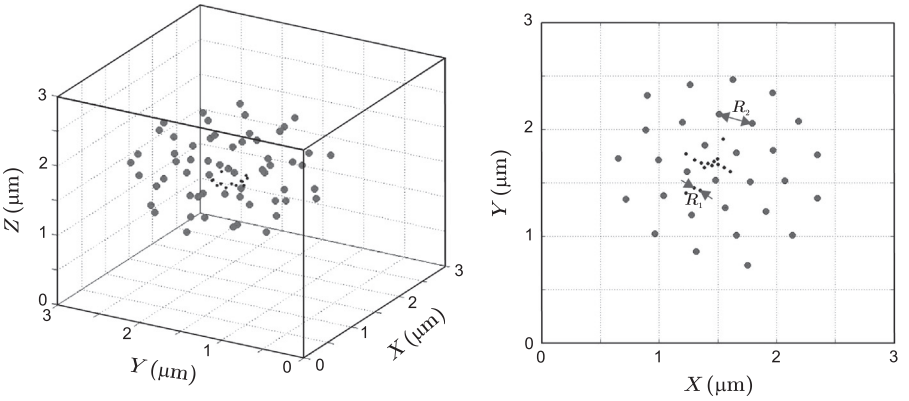

Fig. 1. Examples of 3D and 2D simulations of the primary particles' self-organization.

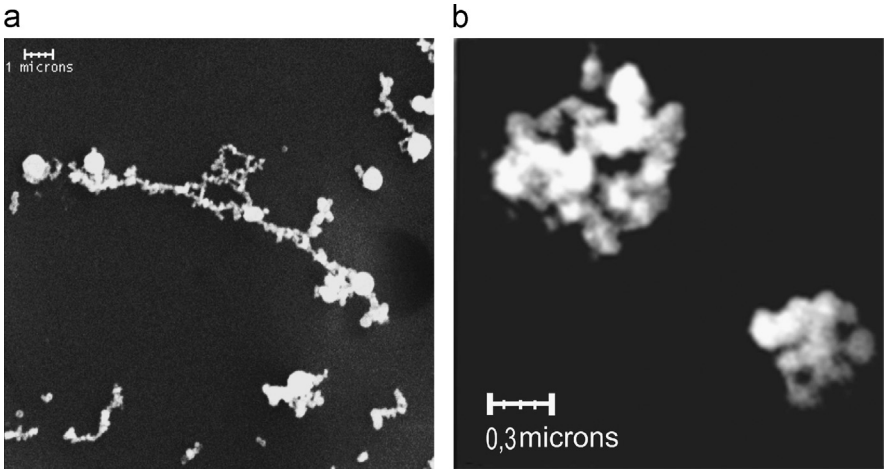

Fig. 2. Aggregates of fine particles: (a) chains, (b) clusters (Oprya et al., 2012).

The number density of the particles of the first mode is much less than of the second one. Therefore, their self-organization creates the structures into only some cells of the plasma crystal of the second mode. The average distance between particles in this structure is $R_1 \sim 0.05$ μm, that ensures their local number density of $n_{d1}^* \sim 10^{16}$ cm^{-3}. The time of such a structure formation is ~ 0.1 μs.

Thus, the self-organization of the dusty plasma of welding fumes leads to increasing of the local number density of the primary particles up to values when their rapid coagulation becomes possible. It should be noted that congestions of the first-mode particles contain about 100–200 particles, and all they create a single agglomerate.

The agglomerates formed in the welding fumes, when the electrodes with carbonate–fluorite coating (Paton UONI) were used, are demonstrated in the photomicrographs of Fig. 2. There are two basic types of the agglomerates: chain-like and cluster-like spatial structures. The agglomerates of the first type are formed by the coagulation of the first-mode particles, as it follows from the result of modeling (see Fig. 1).

4. Collision kernel

The evolution of the number density of agglomerates of size j by coagulation due to the Brownian motion is described by the Smoluchowski balance equation (Bilodeau & Proulx, 1996):

$$\frac{\partial N_j}{\partial t} = \frac{1}{2}\sum_{i=1}^{j-1} \beta_{i,j-i} N_i N_{j-i} - N_j \sum_{i=1}^{\infty} \beta_{i,j} N_i, \tag{8}$$

where $\beta_{i,j}$ is the collision kernel; N_j and N_i are the number densities of the colliding particles.

The Brownian collision kernel can be determined by the kinetic theory of gases, or by the diffusion theory according to the particle size. If the particles are much smaller than mean free path length of the gas molecules, the kinetic theory of gases must be used to determine the collision kernel: $\beta_{i,j} = \sigma_{i,j} v$, where $\sigma_{i,j}$ is the average collision cross-section; v is the relative velocity of the particles. The interaction between particles influences the collision cross-section, which can be described in the following form (Olevanov et al., 2004):

$$\sigma_{i,j} = \sigma_0 \left(1 - \frac{2U_{i,j}}{\mu v^2}\right), \quad \sigma_0 = \pi (a_i + a_j)^2 \tag{9}$$

where $\mu = m_i m_j/(m_i + m_j)$ is the reduced mass of the particles; a_i and a_j are their radii; $U_{i,j}$ is the interaction energy on the shortest distance between the interacting particles. In the system under consideration the particles always repel each other on the short distance: likely charged particles are repelled by the electrical force, and unlikely charged particles are repelled by the ion pressure force.

The collision kernel is $\beta_{i,j} = \langle \sigma_{i,j} v_{i,j} \rangle$, where the averaging is performed over the relative velocities of the particles. Then, under the assumption of the Maxwellian distribution, for the repellent particles it follows:

$$\beta_{i,j} = 4\pi\sigma_0 \left(\frac{\mu}{2\pi k_B T}\right)^{3/2} \int_{v_0}^{\infty} \left(1 - \frac{2U_{i,j}}{\mu v^2}\right) \exp\left(-\frac{\mu v^2}{2k_B T}\right) v^3 \, dv, \tag{10}$$

where $v_0 = \sqrt{2U_{i,j}/\mu}$ is the minimum relative velocity of the particles at which they can collide.

Integrating over velocities yields

$$\beta_{i,j} = \sigma_0 \sqrt{\frac{8k_B T}{\pi\mu}} \exp\frac{-U_{i,j}}{k_B T}. \tag{11}$$

The agglomerates generated from the solid primary particles are the irregular structures; therefore the radius of agglomerate which contains n primary particles (monomers) is described as

$$a = a_0 n^{1/D_f},$$

where D_f is the fractal dimension ($D_f = 3$ for a perfect sphere), a_0 is the radius of the monomers. And in this case the collision kernel for the free molecule regime without interaction between the particles is described by the following equation (Wu & Friedlander, 1992):

$$\beta_{n,m}^0 = \sqrt{\frac{6k_B T a_0}{\rho}} \sqrt{\frac{1}{n} + \frac{1}{m}} (n^{1/D_f} + m^{1/D_f})^2, \tag{12}$$

where ρ is the density of the monomers; n and m are their number per agglomerate with fractal dimension D_f.

In the system under consideration the distance between particles is much less than the screening length. Therefore, the particle electrical interaction can be considered in the Coulomb approximation,

$$U_{n,m} = \frac{(eZ_0)^2 (nm)^{1/D_f}}{a_0 (n^{1/D_f} + m^{1/D_f})}, \tag{13}$$

where Z_0 is the charge number of the primary particle.

Then the collision kernel for the particles which repel each other by the electrical force is

$$\beta_{n,m}=\sqrt{\frac{6k_BTa_0}{\rho}}\sqrt{\frac{1}{n}+\frac{1}{m}}(n^{1/D_f}+m^{1/D_f})^2\exp\left[-\frac{(eZ_0)^2(nm)^{1/D_f}}{a_0(n^{1/D_f}+m^{1/D_f})k_BT}\right]. \tag{14}$$

5. Method of moments

The coagulation equation (8) in its integrodifferential form reads

$$\frac{df_n}{dt}=\frac{1}{2}\int_0^n \beta_{n-m,m}f_{n-m}f_m\,dm-f_n\int_0^\infty \beta_{n,m}f_m\,dm, \tag{15}$$

where f_n is the probability density function based on the number of monomers (primary particles) contained in the agglomerate:

$$f_n=\frac{n_d}{n\sqrt{2\pi}\ln\sigma}\exp\frac{-(\ln n-\ln n_0)^2}{2\ln^2\sigma}; \tag{16}$$

σ is the standard deviation; $n_0=\overline{n}\exp(-\ln^2\sigma/2)$ is the median of distribution; $\overline{n}$ is the average number of monomers in the agglomerate (the description of agglomerate distribution in welding fumes by the lognormal function has been demonstrated in the paper by Ennan et al., 2013).

The "method of moments" approach to modeling the particle coagulation offers an alternative way to solving the full coagulation equation. The motivation behind using the moments method is to avoid the computational cost inherent in Eq. (15) which requires calculation of the convolution integral at every location and at every time step (Estrada & Cuzzi, 2008). The moment $M(k)$ of the distribution (16) is defined as

$$M(k)=\int_0^\infty n^k f_n\,dn. \tag{17}$$

The zeroth moment represents the total number density of the generated agglomerates, while the first moment corresponds to the total number of monomers in these. The second moment is proportional to the light scattered by the agglomerates in case where their size is much smaller than the wavelength of the incident light (Colombo, Ghedini, Gherardi, Sanibondi, & Shigeta, 2012). Evolution of the moments (17) is described by the following equation (Yu, Lin, & Chan, 2008):

$$\frac{dM(k)}{dt}=\frac{1}{2}\int_0^\infty f_n\int_0^\infty \beta_{n,m}f_m\left[(n+m)^k-n^k-m^k\right]\,dm\,dn. \tag{18}$$

Thus, the average number monomers into the agglomerate are

$$\overline{n}=\frac{M(1)}{M(0)}, \tag{19}$$

and the standard deviation is

$$\sigma=\exp\sqrt{\ln\frac{M(2)M(0)}{M(1)^2}}. \tag{20}$$

The moments (17) and their evolutions (18) are calculated in the "PTC Mathcad Prime 3", where there is a possibility of the defined integrals solving (the description of the solving procedure is represented in paper by Vishnyakov, Kiro, & Ennan, 2014a).

6. Coagulation of the primary particles

The coagulation of the primary particles occurs in the cooling environment that causes decrease of the ionization degree which influences the particle charge. The change in the temperature of the system can be described by the following expression:

$$T(t)=T_\infty+(T_0-T_\infty)\exp(-\alpha_T t), \tag{21}$$

where $T_\infty=300$ K is the ambient air temperature; $T_0=1770$ K is the iron melting point corresponding to the start of the primary particles coagulation; $\alpha_T=400\ \mathrm{s}^{-1}$ is the factor, which is defined by initial conditions of the efflux of vapor from the arc zone (Vishnyakov et al., 2014b).

The dependency of the ion number density on the temperature is presented in Fig. 3. The thermal ionization is negligibly low at the temperature below 1300 K, but the ionization by UV-radiation still exists and is the basic in this case. Besides, the decreasing of the ionizable atom number density under cooling and expansion of the vapor flux should be taken into account. Therefore, an ion effect on the charging of particles can be neglected at the temperature less than 400 K.

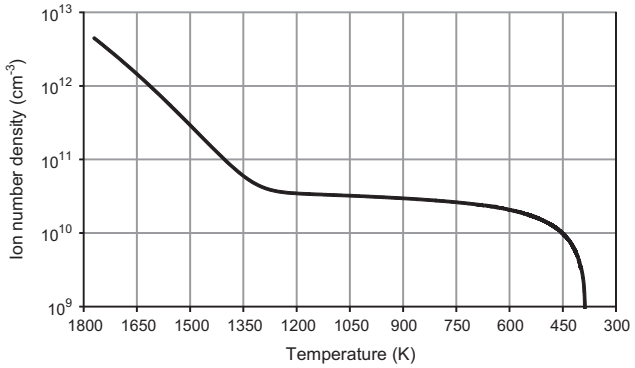

Fig. 3. Dependency of ion number density on the temperature.

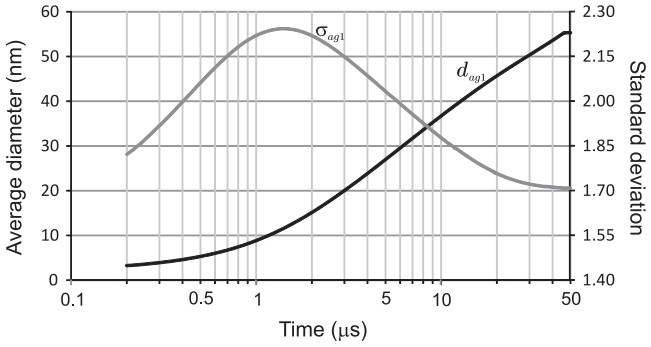

Fig. 4. Evolutions of first-mode agglomerate average size (black) and standard deviation (gray).

The coagulation of the primary particles of the first mode occurs in the local congestions, which are the result of the plasma self-organization. These particles form the chain-like structures corresponding to the fractal dimension $D_{f1} \sim 1.6$ (Eggersdorfer & Pratsinis, 2013). The evolutions of the first-mode agglomerate average sizes and the standard deviation of their lognormal distribution are presented in Fig. 4. The duration of all this process is 50 μs which corresponds to the cooling down to 1735 K. The final average size of the first-mode agglomerates $d_{ag1} = 56$ nm; their number density $n_{ag1} = 2.5 \times 10^9$ cm^{-3}; the standard deviation $\sigma_{ag1} = 1.7$; the mass density $\rho_{ag1} = 0.065$ g/cm^3; and the charge number $Z_{ag1} = -40$.

The evolutions of the agglomerate average sizes and the standard deviation of the lognormal distribution of the second mode under cooling down to 350 K are presented in Fig. 5. The evolution of the agglomerate average charge is presented in Fig. 6. The duration of the basic agglomerate formation is ~ 4 ms under cooling of the system down to 600 K. The final average size of the second-mode agglomerates $d_{ag2} = 230$ nm with fractal dimension $D_{f2} = 2.3$, which completely corresponds to the experimental data (Ennan et al., 2013). The number density of the second-mode agglomerates $n_{ag2} = 5 \times 10^9$ cm^{-3}; the standard deviation $\sigma_{ag1} = 1.5$; and the mass density $\rho_{ag1} = 0.8$ g/cm^3. The agglomerate average charge is increased with the size growth up to $Z_{ag2} = 140$, but is decreased down to $Z_{ag2} = 50$ under cooling of the system below 1100 K.

Here it is necessary to pay some attention to the particle charge, which is formally composed of two parts: $Z = Z_0 + \tilde{Z}$. The first part of charge ($Z_0 = n_0/n_d$, where n_d is the total dust number density) and the unperturbed electrons neutralize each other and create the neutralized background which determines the bulk plasma potential. This part is identical for all dust particles. The second part ($\tilde{Z}$) is individual for each dust particle. This part of charge defines the particle interaction and creates the potential barrier at the plasma–particle boundary (the detailed description of the dust charge in the plasma is represented in the paper by Vishnyakov, 2012). A situation often takes place when the individual part of the charge is opposite to the total particle charge. The individual part of the charge was used in Sections 2 and 3, because this one determines the long-range interaction. However, the total particle charge should be used for characterization of the Coulomb interaction of the colliding particles.

Thus, the agglomerates of the different modes have opposite signs of the charge that causes the intermodal coagulation. In this case the collision cross-section is increased. The collision kernel should be described in the diffusion regime, because the Knudsen number $Kn = \lambda/a < 1$ for agglomerates:

$$\beta_{i,j} = \frac{2k_B T C(a_{i,j})}{3\eta} \frac{(a_i + a_j)}{a_{i,j}} \left(1 + \frac{e^2 |Z_i Z_j|}{(a_i + a_j) k_B T}\right), \tag{22}$$

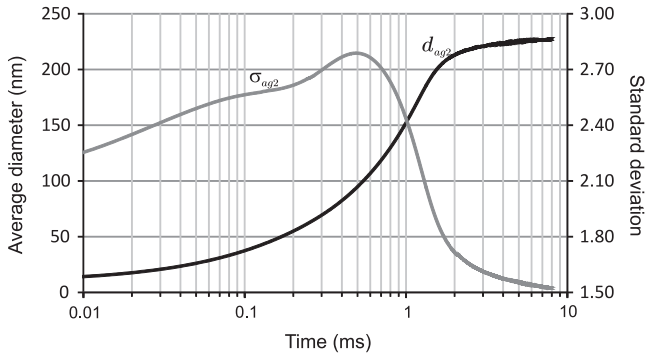

Fig. 5. Evolutions of second-mode agglomerate average size (black) and standard deviation (gray).

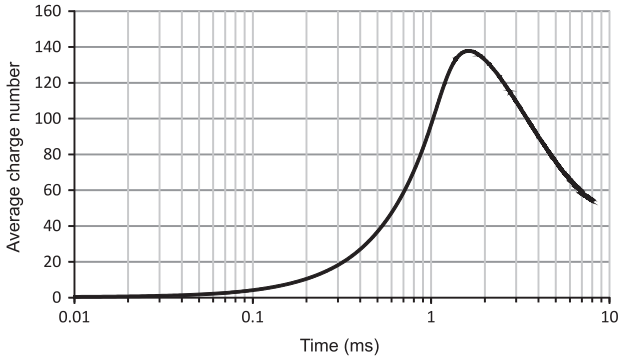

Fig. 6. Evolution of second-mode agglomerate average charge number.

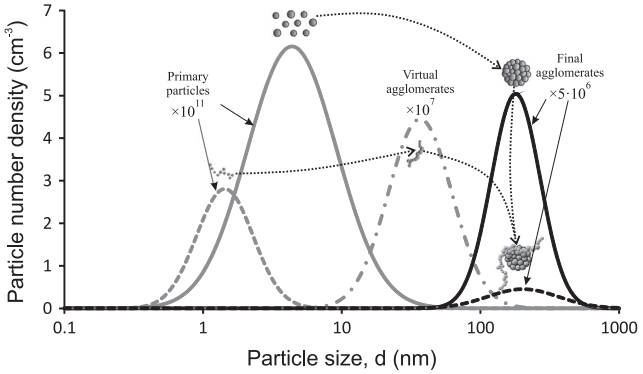

Fig. 7. Number based particle distributions for welding fume when the electrodes Paton UONI are used.

where $a_{i,j} = a_i a_j/(a_i + a_j)$; η is the viscosity; $C(a)$ is the Canningham slip correction (Hagwood, Sivathanu, & Mulholland, 1999)

$$C(a) = 1 + \frac{\lambda}{a}\left(1.142 + 0.588\,\exp\frac{-a}{\lambda}\right);$$

$\lambda = 67$ nm is the mean free path.

The coagulation time, at which the initial number of particles is reduced twice, in this case is ~ 0.1 μs, i.e. the very rapid coagulation takes place. Thus, the intermodal coagulation rate is determined only by the rate of second-mode charge growth. Thus, formation of the new aggregates, which consist of the single second-mode cluster and two or three chains of the first mode, occurs in the process of the second-mode charge growth. Such coagulation leads to neutralizing the charges that causes decreasing of the collision cross-section and termination of the intermodal coagulation. The average diameter of the new aggregates $d_{ag3} \sim 340$ nm, and number density $n_{ag3} \sim 8 \times 10^8$ cm^{-3}.

Thus, the chain-like agglomerates of the first mode exist as self-contained units only short time, i.e. they can be considered as virtual, because their coagulation with the second mode occurs (Fig. 7). The number of second-mode clusters decreases a little – by about 10%. As a result, only two types of the final agglomerates (inhalable particles) remain in the welding fume after cooling: the clusters of primary particles with the average size about 230 nm and the intermodal

aggregates with the average size about 340 nm, whose contents correlate as 85% and 15%, respectively. This result completely corresponds to the experimental data for the welding fumes, when the electrodes with carbonate–fluorite coating (Paton UONI) were used (Ennan et al., 2013).

7. Chemical composition of agglomerates

The multicomponent condensation in the welding fumes causes complex chemical composition of the primary particles (Vishnyakov et al., 2014b). The replacing of iron by low-boiling components in the particles of the first mode with size 2 nm occurs – the content of calcium reaches up to 90% in these, when the electrodes Paton UONI are used. In the primary particles of the second mode the content of iron is reduced down to 60% and content of silicon reaches up to 35%. It means, that content of the components in the intermodal aggregates with average size 340 nm, which consist of the single cluster and several chains, can be in the following ranges: iron of 35–60%, silicon of 10–20%, calcium of 20–30%, and manganese of 10–15%. The final agglomerates with average size 230 nm should consist of 50–65% of iron, 20–30% of silicon, 5–10% of manganese, and 5–10% of calcium.

The elemental composition of the individual welding fume particles was investigated by the Jeol 733 electron-probe microanalysis device, equipped with a super-atmospheric thin window Oxford energy-dispersive X-ray detector (Oprya et al., 2012). The samples for these measurements were collected by a Berner cascade impactor in the welding fumes, when electrodes covered by rutile Paton ANO-4 and carbonate–fluorite Paton UONI have been used. The following results were obtained for the electrodes Paton UONI.

The impactor stage with cut-off aerodynamic diameter of 250 nm contains 60% of the total number of particles which contain 60% of iron, 20% of silicon, 5% of calcium, and 15% of manganese (here and below for calculation of the element composition only the initial elements in the primary particles are considered, i.e. only iron, silicon, manganese and calcium without oxygen, chlorine, etc.). Also, it contains 11% of the total number of particles which contain 65% of iron and 35% of silicon. And also it contains 7% of the total number of particles which contain 50% of iron, 14% of silicon, 21% of calcium, and 15% of manganese. The two first items of this list are the cluster-like agglomerates of the second mode with the average diameter of 230 nm; and the latter is, probably, the composite aggregates with single cluster and single chain, whose diameter is about 280 nm.

The impactor stage with cut-off aerodynamic diameter of 500 nm contains 60% of the total number of particles which contain 45% of iron, 25% of silicon, 15% of calcium, and 15% of manganese. These particles represent the intermodal aggregates of the single cluster and three chains with the average diameter of 340 nm. This impactor stage also contains 0.3% of the total number of particles which consist only of low-boiling components: 65% of calcium and 35% of manganese; and they, most likely, represent the aggregates of the chains without clusters. The rest of the particles in this stage contains only iron ($>50\%$) and silicon, and represents the cluster-like agglomerates from the tail of the lognormal distribution with the average diameter of 230 nm.

Thus, the calculations of the chemical composition of the primary particles represented by Vishnyakov et al. (2014b) and the presented above calculations of the coagulation in the self-organizing plasma of the welding fume, when electrodes with carbonate–fluorite coating (Paton UONI) are used, completely correspond to the experimental data of their disperse (Ennan et al., 2013) and chemical compositions (Oprya et al., 2012).

8. Conclusion

The dusty plasma of welding fumes at the temperature of the phase transition of condensed liquid droplets into the solid primary particles is the self-organizing system, in which the ordered structures of the primary particles are formed. This process causes the rapid coagulation, because the local number densities of the primary particles in the ordered structures are much higher than at uniform spatial distribution.

The Brownian motion suppresses the plasma self-organization. Formation of the plasma crystals is possible only under the strong potential interaction, when it exceeds the motion energy. Therefore, considered above effects are impossible at the nucleation or the nuclei growth, because small charges of the droplets and the high temperature prevent the plasma crystals formation. However, near the temperature of phase transition the particle surface potentials reach such values that the self-organization becomes possible. Therefore, the formation of ordered structures from the liquid droplets is possible; and rapid coagulation of the droplets and formation of the large solid particles at such temperature are possible too. But it should be taken into account that melting point depends on the particle size and coagulation of the droplets rapidly leads to the phase transition and to the start of the solid particles coagulation.

The increasing of the local number density of primary particles as a result of the ordered structures formation ensures their rapid coagulation. The particles with the size more 10 nm are coagulated into the cluster-like positively charged agglomerates. This process occurs during the cooling of system down to the temperature of ~ 600 K. The fine primary particles with the size about 2 nm are coagulated by two stages: at first the chain-like negatively charged agglomerates are formed during the short time, and then, because the clusters and chains are unlikely charged, they associate with the cluster-like agglomerates. The latter process provides the neutralization of the particle charges. As a result, the final agglomerates (inhalable particles) have the bimodal size distribution with different chemical compositions.

These results well correspond to the experimental data by Sowards et al. (2010), Berlinger et al. (2011), Oprya et al. (2012) and Ennan et al. (2013) where the disperse and chemical compositions of the inhalable particles in welding fumes have been demonstrated.

References

Belov, I.A., Ivanov, A.S., Ivanov, D.A., Pal', A.F., Starostin, A.N., Filippov, A.V., Dem'yanov, A.V., & Petrushevich, Yu.V. (2000). Coagulation of charged particles in a dusty plasma. *Journal of Experimental and Theoretical Physics*, *90*, 93–101.

Belov, I.A., Ivanov, A.S., Pal, A.F., Ryabinkin, A.N., & Serov, A.O. (2002). Effect of selective coagulation of the likely charged particles in a dusty plasma trap. *Physics Letters*, *A306*, 52–56.

Berlinger, B., Benker, N., Weinbruch, S., L'Vov, B., Ebert, M., Koch, W., Ellingsen, D.G., & Thomassen, Y. (2011). Physicochemical characterisation of different welding aerosols. *Analytical and Bioanalytical Chemistry*, *399*(5), 1773–1780.

Bilodeau, J.-F., & Proulx, P. (1996). A mathematical model for ultrafine iron powder growth in a thermal plasma. *Aerosol Science and Technology*, *24*, 175–189.

Bouchoule, A., Boufendi, L., Hermann, J., Plain, A., Hbid, T., Kroesen, G., Stoffels, E., & Stoffels, W.W. (1996). Formation of dense submicron clouds in low pressure Ar–SiH_4 RF reactor: Diagnostics and growth processes from monomers to large size particles. *Pure and Applied Chemistry*, *68*, 1121–1126.

Colombo, V., Ghedini, E., Gherardi, M., Sanibondi, P., & Shigeta, M. (2012). A two-dimensional nodal model with turbulent effects for the synthesis of Si nano-particles by inductively coupled thermal plasmas. *Plasma Sources Science and Technology*, *21*(1–12), 025001.

Eggersdorfer, M.L., & Pratsinis, S.E. (2013). The structure of agglomerates consisting of polydisperse particles. *Aerosol Science and Technology*, *46*, 347–353.

Ennan, A.A., Kiro, S.A., Oprya, M.V., & Vishnyakov, V.I. (2013). Particle size distribution of welding fume and its dependency on conditions of shielded metal arc welding. *Journal of Aerosol Science*, *64*, 103–110.

Estrada, P.R., & Cuzzi, J.N. (2008). Solving the coagulation equation by the moment method. *The Astrophysical Journal*, *682*, 515–526.

Fortov, V.E., Khrapak, A.G., Khrapak, S.A., Molotkov, V.I., & Petrov, O.F. (2004). Dusty plasmas. *Physics–Uspekhi*, *47*, 447–492.

Hagwood, Ch., Sivathanu, Yu., & Mulholland, G. (1999). The DMA transfer function with Brownian motion a trajectory/Monte-Carlo approach. *Aerosol Science and Technology*, *30*, 40–61.

Ivlev, A.V., Morfill, G.E., & Konopka, U. (2002). Coagulation of charged microparticles in neutral gas and charge-induced gel transition. *Physical Review Letters*, *89*(1–4), 195502.

Khrapak, S.A., Ivlev, A.V., Morfill, G.E., & Thomas, H.M. (2002). Ion drag force in complex plasmas. *Physical Review E*, *66*(1–4), 046414.

Landau, L.D., & Lifshitz, E.M., (1976). Statisticheskaya Fizika (Statistical Physics) (Vol. 1). Nauka: Moscow (translated into English 1980, Pergamon: Oxford).

Mankelevich, Yu.A., Olevanov, M.A., Pal', A.F., Rakhimova, T.V., Ryabinkin, A.N., Serov, A.O., & Fillipov, A.V. (2009). Coagulation of dust grains in the plasma of an RF discharge in argon. *Plasma Physics Report*, *35*, 191–199.

Morfill, G.E., Khrapak, S.A., Ivlev, A.V., Klumov, B.A., Rubin-Zuzic, M., & Thomas, H.M. (2004). From fluid flows to crystallization: New results from complex plasmas. *Physica Scripta*, *T107*, 59–64.

Morfill, G.E., Thomas, H.M., Konopka, U., & Zuzic, M. (1999). The plasma condensation: Liquid and crystalline plasmas. *Physics of Plasmas*, *6*, 1769–1780.

Nguyen, T.T., & Shklovskii, B.I. (2002). Kinetics of macroion coagulation induced by multivalent counterions. *Physical Review E*, *65*(1–7), 031409.

Olevanov, M.A., Mankelevich, Yu.A., & Rakhimova, T.V. (2003). Coagulation rate of dust grains in a low-temperature plasma. *Technical Physics*, *48*, 1270–1279.

Olevanov, M.A., Mankelevich, Yu.A., & Rakhimova, T.V. (2004). Coagulation and growth mechanisms for dust particles in a low-temperature plasma. *Journal of Experimental and Theoretical Physics*, *98*, 287–304.

Oprya, M., Kiro, S., Worobiec, A., Horemans, B., Darchuk, L., Novakovic, V., Ennan, A., & Van Grieken, R. (2012). Size distribution and chemical properties of welding fumes of inhalable particles. *Journal of Aerosol Science*, *45*, 50–57.

Smith, M., Lee, K., & Matsoukas, T. (1999). Coagulation of charged aerosols. *Journal of Nanoparticle Research*, *1*, 185–195.

Sowards, J.W., Ramirez, A.J., Dickinson, D.W., & Lippold, J.C. (2010). Characterization of welding fume from SMAW electrodes—Part 2. *Welding Journal*, *89*, 82s–90s.

Vishnyakov, V.I. (2004). The bulk plasma potential as a tool for the description of the interaction of dust grains. *Ukrainian Journal of Physics*, *50*, 200–204.

Vishnyakov, V.I. (2005). Interaction of dust grains in strong collision plasmas: Diffusion pressure of nonequilibrium charge carriers. *Physics of Plasmas 12*(1–6), 103502.

Vishnyakov, V.I. (2006). Electron and ion number densities in the space charge layer in thermal plasmas. *Physics of Plasmas*, *13*(1–4), 033507.

Vishnyakov, V.I. (2012). Charging of dust in thermal collisional plasmas. *Physical Review E*, *85*(1–6), 026402.

Vishnyakov, V.I., & Dragan, G.S. (2005). Electrostatic interaction of charged planes in the thermal collision plasma: Detailed investigation and comparison with experiment. *Physical Review E*, *71*(1–9), 016411.

Vishnyakov, V.I., & Dragan, G.S. (2006). Ordered spatial structures of dust grains in the thermal plasma. *Physical Review E*, *73*(1–7), 026403.

Vishnyakov, V.I., Kiro, S.A., & Ennan, A.A. (2014a). Bimodal size distribution of primary particles in the plasma of welding fume: Coalescence of nuclei. *Journal of Aerosol Science*, *67*, 13–20.

Vishnyakov, V.I., Kiro, S.A., & Ennan, A.A. (2014b). Multicomponent condensation in the plasma of welding fumes. *Journal of Aerosol Science*, *74*, 1–10.

Watanabe, Y. (2006). Formation and behaviour of nano/micro-particles in low pressure plasmas. *Journal of Physics D: Applied Physics*, *39*, R329–R361.

Wu, M.K., & Friedlander, S.K. (1992). Enhanced power law agglomerate growth in the free molecule regime. *Journal of Aerosol Science*, *24*, 273–282.

Yu, M., Lin, J., & Chan, T. (2008). A new moment method for solving coagulation equation for particles in Brownian motion. *Aerosol Science and Technology*, *42*, 705–713.

Zimmer, A.T., & Biswas, P. (2001). Characterization of the aerosols resulting from arc welding processes. *Journal of Aerosol Science*, *32*, 993–1008.